Welding in the World (2025) 69:825–836
https://doi.org/10.1007/s40194-024-01908-0

RESEARCH PAPER

Physical simulation-based analysis of multipass welding in S500 shipbuilding steel

M. Gáspár[1] · J. Kovács[1] · J. Sainio[2] · H. Tervo[3] · V. Javaheri[3] · A. Kaijalainen[3]

Received: 28 August 2024 / Accepted: 2 December 2024 / Published online: 14 December 2024

Abstract
Novel generations of shipbuilding steels have outstanding toughness due to the improved steel producing processes. Their microstructure mainly consists of ferrite and bainite, while the presence of acicular ferrite has a role in high impact energy of the welded joint. This research aims to analyze the effect of multipass welding on weld characteristics of S500 shipbuilding steel. A Gleeble 3500 simulator machine is used to produce the welding thermal cycles by the Rykalin-3D model on 70 × 10 × 10 mm samples manufactured in transversal direction from a submerged arc welded joint of 16 mm plate. Temperatures for the simulations were set at 1350 °C for the coarse-grained zone forming in the weld metal (CGHAZ-W), 815 °C for the intercritical zone (ICHAZ-W), and a combination of these peak temperatures for the intercritically reheated coarse-grained zone (ICCGHAZ-W). The examined $t_{8/5}$ interval was 5–30 s. The weld properties were examined by microstructural examination, hardness test, and instrumented Charpy V-notch impact toughness test. The impact energy values of subzones were below the unaffected weld metal. Longer cooling time resulted in lower impact energy in ICHAZ-W. However, this tendency was not observed in CGHAZ-W. ICHAZ-W and ICCGHAZ-W resulted in the lowest impact toughness, which was indicated by the large unstable crack propagation.

Keywords S500 shipbuilding steel · Physical simulation · Welding · Instrumented impact test · Microstructural characterization

1 Introduction

Modern low-carbon thermomechanically manufactured steels are popularly used in shipbuilding and marine structures (oil rigs, foundations for wind turbines), where the components of the product must withstand extreme environmental load and the resulting increased mechanical stress [1]. These structures are often subjected to dynamic loading at negative temperatures. Therefore, the steel producers strive to provide these steels with excellent toughness properties in response to strict regulations. Depending on the steel grades, offshore steels are produced by normalizing (N), thermomechanically controlled processing (TMCP), or quenching and tempering (Q + T). The TMCP steels in the medium strength range (R_{eH} = 400–500 MPa) are characterized by low carbon content and low carbon equivalent (CE) with the mixed microstructure of ferrite and bainite. Offshore steels with the highest toughness are typically manufactured by TMCP, which leads to an extremely fine-grained microstructure [2, 3]. In welded joints, the presence of acicular ferrite (AF) forming across the small precipitates and

Recommended for publication by Commission IX - Behaviour of Metals Subjected to Welding

✉ M. Gáspár
marcell.gaspar@uni-miskolc.hu

J. Kovács
judit.kovacs@uni-miskolc.hu

J. Sainio
johannes.sainio@ssab.com

H. Tervo
henri.tervo@oulu.fi

V. Javaheri
vahid.javaheri@oulu.fi

A. Kaijalainen
antti.kaijalainen@oulu.fi

1 University of Miskolc, Miskolc, Hungary

2 SSAB Europe/Knowledge Center, Raahe, Finland

3 University of Oulu, Oulu, Finland

inclusions has a determining role in achieving the demanded toughness [2]. However, the presence of martensite-austenite (M-A) constituents can reduce the impact energy especially in the heat-affected zone [4]. Due to the favorable chemical composition, these steels have good weldability, which is verified by their location in the first zone of the Graville diagram [5]. Cold cracking is not expected to occur; however, it may initiate in larger cross sections from the existing hot cracks at the end crater [6]. Deterioration of toughness in the HAZ is a known problem with offshore steels [3, 7]. Furthermore, it is a challenge to guarantee that the impact energy level in the dendritic, mostly multipass weld is the same as that in the fine-grained and micro-alloyed steel plate, which is rolled through specific rolling processes. The applied standards [8] have certain acceptance criteria for the toughness properties of the HAZ and the weld, which are typically required to be tested with Charpy V-notch (CVN) impact tests and with fracture toughness tests, such as crack-tip opening displacement (CTOD). Nowadays, numerous studies deal with the role of AF in the heat-affected zone (HAZ) [7, 9]. However, there is less focus on the weld microstructure and mechanical properties.

The effects of titanium content on the weld microstructure, mechanical properties, and inclusion characteristics were investigated by Seo et al. [10] in as-deposited bainitic gas metal arc weld metals having a nearly constant level of oxygen content. It was found that titanium addition enhanced the formation of AF, with the maximum proportion being obtained at ~0.07 wt.% Ti. The resultant change in weld microstructure with titanium content was well reflected in the Charpy impact energy, showing the lowest ductile–brittle transition temperature at 0.07 wt.% Ti.

The effect of multipass welding on the weld metal was studied previously, e.g., by Kang et al. [11]. They utilized physical simulation to study the microstructures and mechanical properties in reheated zones in two different weld metals. They concluded that the toughness reduction in reheated zones of low hardenability weld metal was attributed to the increase of grain boundary ferrite in the microstructure, whereas in the high hardenability weld metal, the reason for the reduced toughness in the reheated zones was coalesced bainite.

Multipass weld metal microstructures of 420 MPa offshore steel was studied by Nellikode et al. [12]. In their study instead of physical simulation, the investigation was about reheated zones (RHZ) in actual welds. The welding was performed using three different heat inputs, which affected the required number of passes. Each weld was divided into different sections based on the local fraction of RHZs in the microstructure. According to their analysis, the initial columnar prior austenite grains were refined to equiaxial grains in RHZs and the fraction of polygonal ferrite, quasi-polygonal ferrite, grain boundary ferrite, bainite, and martensite-austenite constituents increased, whereas the fraction of AF decreased. They concluded that the highest impact toughness was obtained in sections where the fraction of AF was high. The highest risk for the deterioration of impact toughness was suggested when welding multiple passes with high heat input.

Actual welds were also studied by Bhole et al. [13], but of high strength low alloy (HSLA) steels. According to their study, the increasing fractions of AF and granular bainite improve impact toughness of the weld metal, whereas high fractions of grain boundary ferrite and ferrite with second phase decrease the impact toughness.

Finally, as noted by Abson [14], there has been a lot of confusion between intragranularly nucleated AF and bainite in C-Mn and low alloyed steel weld metals since they look very similar in optical micrographs. Therefore, it is crucial to utilize sufficiently high magnification microscopy, e.g., scanning electron microscopy (SEM), for reliable microstructural characterization in such weld metals.

The goal of the present research is to investigate the properties of a multipass welded joint of a 500 MPa grade shipbuilding steel by physical simulation in the industrially relevant $t_{8/5}$ cooling time range of arc welding processes. The experimental program is aimed at the production and analysis of physically simulated HAZ subzones (coarse-grained, intercritical, intercritically reheated coarse-grained) occurring in the weld, which can be considered critical zones in terms of toughness, using microstructural characterization, hardness test, and instrumented Charpy V-notch impact toughness test.

2 Experimental

2.1 Base and filler materials

Table 1 summarizes the chemical composition of the 500 MPa grade (S500ML) shipbuilding steel, classified by EN 10025–4 [15], the selected S3Ni1Mo0.2 according to EN ISO 14171 [16] filler metal for submerged arc welding (SAW), and the weld. In the case of the base material, which is under development, the publication of the exact chemical composition was not allowed. The copper-coated wire electrode is alloyed by nickel and molybdenum with a diameter of 4 mm which is qualified by CTOD (crack tip opening displacement) tests. The recommended flux for the given filler material is EN ISO 14174: S A FB 1 55 AC H5, which is a high basicity, neutral, bonded flux intended primarily for multipass butt welding of carbon and low alloy steel plates. It produces weld metal that is very clean metallurgically and exhibits exceptional impact toughness at low temperatures. This filler material and flux combination is

Table 1 Chemical compositions of the base, filler material, and the weld

Material	C	Si	Mn	P	S	Cr	Mo	Ni	Nb	V	Ti	Cu	Al	B	CEV	CET
Base material	≤0.14	≤0.6	≤1.7	≤0.02	≤0.01	Cr + Mo ≤ 0.65		≤2.0	Nb + V + Ti ≤ 0.26			≤0.55	≥0.02	N/A	N/A	N/A
Filler material	0.067	0.184	1.33	0.015	0.0078	0.053	0.187	0.784	0.003	0.003	0.003	0.058	0.014	0.002	0.49	0.27
Weld*	0.053	0.366	1.46	0.011	0.0058	0.061	0.201	0.893	0.024	0.006	0.007	0.202	0.022	0.0002	0.42	0.25

*Optical emission spectrometer (OES) analysis

Table 2 Mechanical properties of the base and filler material

Material	R_{eH}, MPa	R_m, MPa	A_5, %	CVN, J
Base material	500	580–760	15	20 J [− 40 °C]
Filler material	530	620	N/A	N/A

directly developed for fine grained steels in offshore industry and shipbuilding.

The guaranteed mechanical properties of the base and filler material are summarized in Table 2.

2.2 Gleeble simulation

In contrary to the conventional application of Gleeble physical simulators for the HAZ tests [17, 18], the goal of present experiments was the simulation-based analysis of multipass welding heat cycles on weld properties. For this purpose, welded joints were prepared from 16-mm-thick plates by submerged arc welding (SAW) without pre-heating at room temperature in laboratory conditions using heat input of 5 kJ/mm. SAW was chosen to produce a relatively homogenous weld in one layer, which is sufficient in volume for the production of physical simulation specimens. As shown in Fig. 1, a symmetric one side joint was prepared with a Y-groove, the root gap was 3 mm, the depth of root face was 4 mm, and the angle of bevel was 40°. In terms of the applied welding parameters, the welding current was 751 A, the welding voltage was 30.8 V, the wire feeding speed was 1.75 m/min, the welding speed was 27.9 cm/min, and the welding heat input was 5 kJ/mm. The physical simulation specimens were machined transversely from the welded joint in such a way that the seam falls in the middle part of the specimens. The specimen size was 70 × 10 × 10 mm. The physical simulation experiments were performed on a Gleeble 3500 thermophysical simulator. Using this equipment, the desired subzones of welded joint can be precisely and homogeneously produced in a sufficient volume for the further material tests.

The physical simulation experiments were aimed at producing the most unfavorable microstructure occurring in the multilayer weld in terms of the toughness properties. Therefore, 1350 °C was selected for the simulation of coarse-grained heat-affected zone forming in the weld (CGHAZ-W) and 815 °C peak temperature was used for the intercritical heat-affected zone (ICHAZ-W). In the case of CGHAZ-W, the motivation was to produce the largest possible grains in the heat-affected zone. In the case of the ICHAZ-W, when choosing the temperature, we assumed that the estimated value of the A_{c1} temperature for steels with a low carbon equivalent is 765 °C, and for the intercritical simulation, based on practical experience, it is worth choosing $A_{c1} + 50 = 815$ °C. The combination of the two

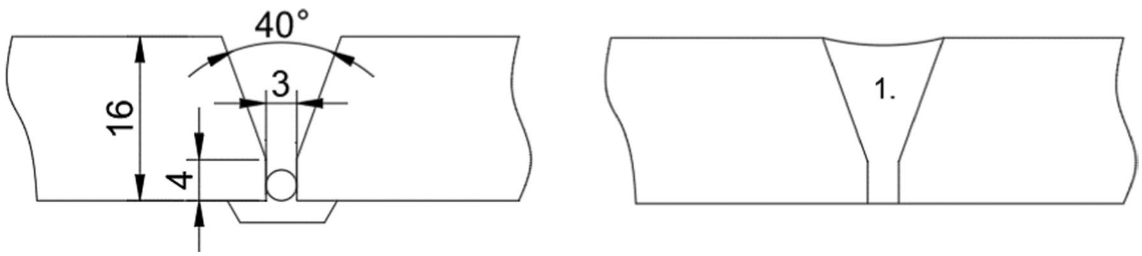

Fig. 1 Joint design and welding sequence

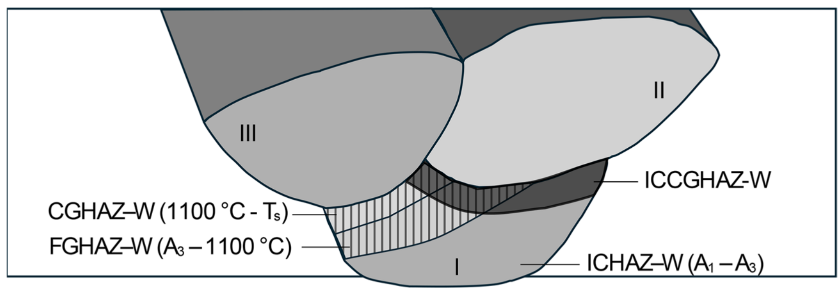

Fig. 2 A part of heat-affected subzones formed in the weld during multipass welding

thermal cycles was applied for the simulation of the local intercritically reheated coarse-grained heat-affected zone (ICCGHAZ-W). Figure 2 illustrates as an example how, in the case of a three-layer weld construction, the different subzones are formed in the weld as a result of the heat effect of each row of weld seams. In the ICCGHAZ-W located in the first welding pass, the grains coarsen due to the heat cycle of the second pass, and then the third weld pass intercritically reheats this area with heating between A_{c1} and A_{c3}.

The examined $t_{8/5}$ interval was 5–30 s, which was chosen considering the characteristic welding heat input of arc welding processes. The Rykalin-3D model [19] was used for the production of heat cycles, which was set by the thermophysical properties of the investigated 500 MPa carbon steel as follows: density $\rho = 7.7$ g/cm^3, specific heat at constant pressure c_p = 0.46 J/g·°C, and thermal conductivity $\lambda = 0.50$ J/cm·s·°C. Figures 3 and 4 show the CGHAZ-W and ICHAZ-W cycles produced using the Rykalin model. In the case of CGHAZ-W, the heating rate was 1200 °C/s and the holding time at peak temperature was 0.1 s, while in case of ICHAZ-W, the heating rate was 200 °C/s and holding time at peak temperature was 0.5 s. In both thermal cycles, according to Rykalin-3D model, the cooling was stopped at 250 °C, after which the specimens cooled down freely to room temperature in the copper grips. For the simulation of ICCGHAZ-W (Fig. 5), the second cycle started when the first cycle had decreased to 150 °C. A K-type thermocouple was used during the simulations for temperature control and measurement. Thermocouples were welded to the surface at 1 mm distance from the weld centerline in order to avoid the effect of possible segregation.

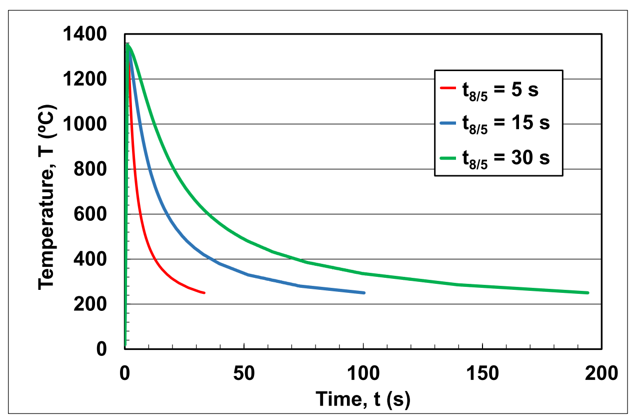

Fig. 3 CGHAZ-W thermal cycles based on the Rykalin-3D model

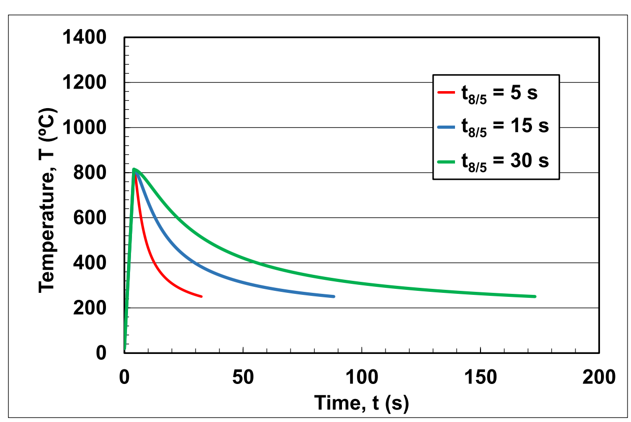

Fig. 4 ICHAZ-W thermal cycles based on the Rykalin-3D model

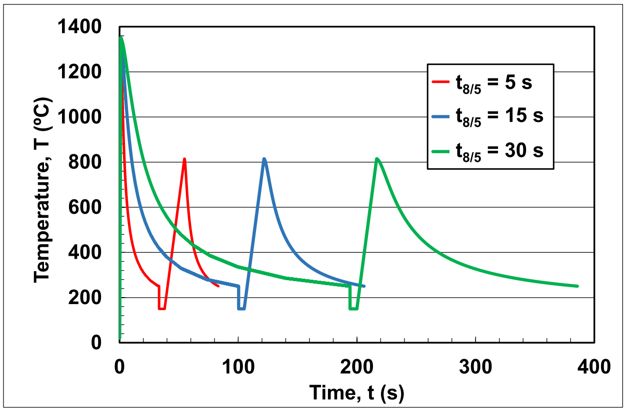

Fig. 5 ICCGHAZ-W thermal cycles based on the Rykalin-3D model

3 Results and discussion

The properties of the simulated HAZ subzones were analyzed by scanning electron microscopy, macroscopic and hardness tests, and the instrumented Charpy V-notch impact test.

3.1 Microstructural characterization

Specimens were mechanically cut at the thermocouples. Then, the surface was grinded and polished before etching with 2% Nital (alcoholic solution containing 2% HNO_3). Detailed observation into the weld metal microstructures was carried out using field emission scanning electron microscopy (FESEM, Zeiss Sigma). The applied acceleration voltage was 5 kV, and the working distance was in the range of 4–6 mm.

Figure 6 shows the as-deposited weld microstructure and the HAZ-W microstructures are shown in Fig. 7. As seen in Fig. 6a, the microstructure of the original weld metal consists mainly of AF, although grain boundary ferrite is also present. The higher magnification image in Fig. 6b shows the AF having nucleated from small (< 1 µm) non-metallic inclusions.

The HAZ-W microstructures (Fig. 7) are presented with the corresponding hardness values of each sample to clarify the change in the microstructure. More detailed analysis of the hardness results will follow in Sect. 3.2.

Generally, it can be observed that the AF microstructure mostly remains in the samples after thermal cycles of HAZ-W simulations. However, in CGHAZ-W simulation with $t_{8/5} = 5$ s, higher degree of hardening was observed among AF (Fig. 7a) due to rapid cooling from temperatures above A_3 where the steel was fully austenitic. Based on their morphology, these features look like upper bainite.

In ICHAZ-W simulations, the amount of martensite-austenite (M-A) constituents increased with increased cooling time. The peak temperature in ICHAZ-W simulations was between A_1 and A_3, meaning that the steel was partly austenitized. Therefore, the initial AF microstructure is still widely present.

In ICCGHAZ-W simulations, initial slight hardening occurred due to the first heat cycle, and M-A constituents were formed as a result of the second heat cycle, similarly to ICHAZ-W simulations. Figure 8 provides a more detailed observation of M-A constituents in ICHAZ-W and ICCGHAZ-W with $t_{8/5}$ of 5 s and 30 s. With slow cooling, there is more time for carbon partitioning from matrix to M-A, and for stabilizing constituents. Therefore, an increased fraction of M-A was detected with increasing cooling time. Additionally, it is noted that ICHAZ-W and ICCGHAZ-W microstructures do not differ remarkably from each other.

3.2 Macroscopic and hardness test

A Reicherter UH250 universal macro hardness tester was used for the hardness measurement. Evaluation was based

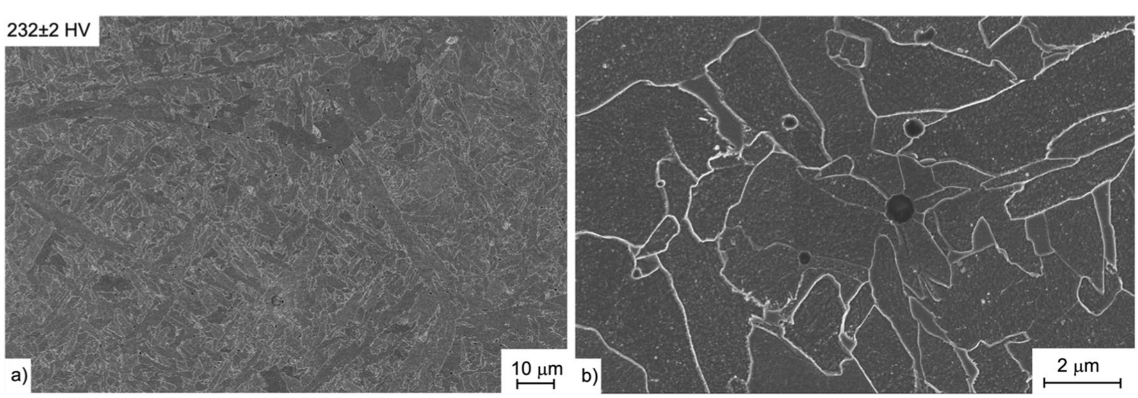

Fig. 6 Scanning electron microscope images of the as-deposited weld microstructure. Overall view of the microstructure consisting of acicular and grain boundary ferrite (**a**). Detail of acicular ferrite laths nucleating from a non-metallic inclusion (**b**)

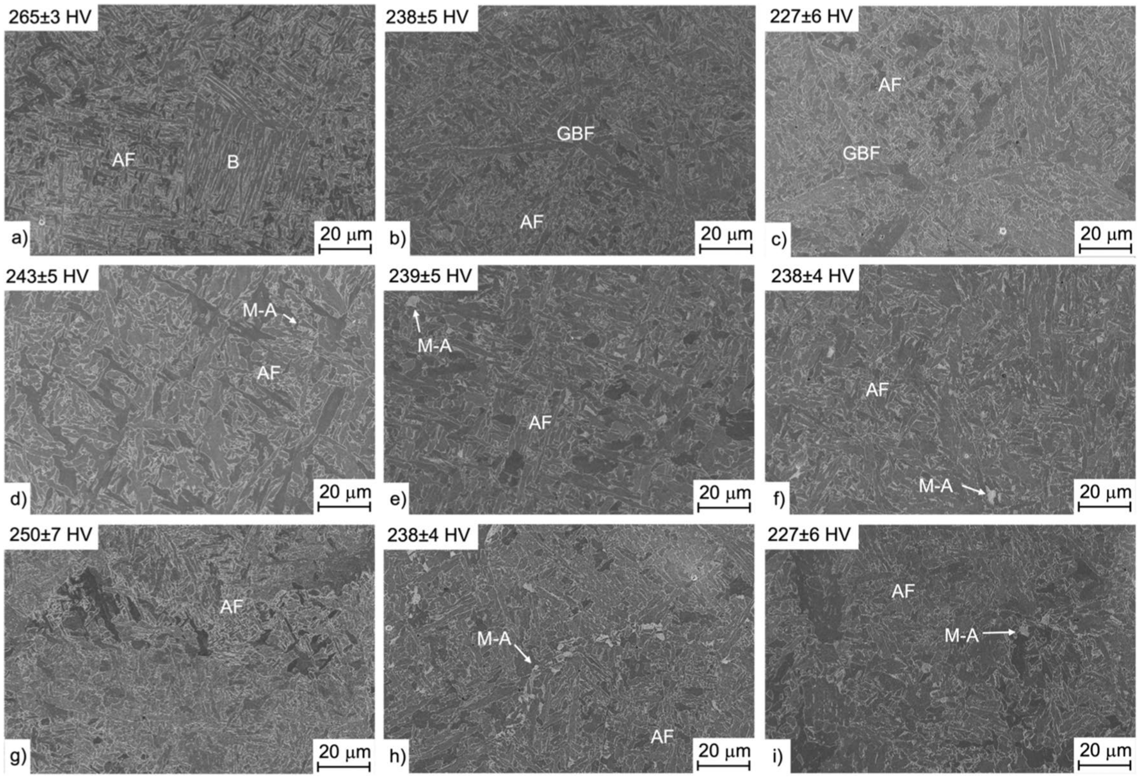

Fig. 7 Scanning electron microscope images and corresponding hardness values of CGHAZ-W (**a**, **b**, **c**), ICHAZ-W (**d**, **e**, **f**), and ICCGHAZ-W (**g**, **h**, **i**) with $t_{8/5} = 5$, 15, and 30 s, respectively. AF, acicular ferrite; B, bainite; GBF, grain boundary ferrite; M-A, martensite-austenite constituent

on the EN ISO 15614–1 [20] welding qualification standard, which allows $HV_{max} = 380$ HV10 hardness for the non-heat-treated welded joints of the thermomechanically controlled processed steels belonging to the 2nd group of CEN ISO/TR 15608 [21]. The measured transversal hardness distribution before the Gleeble simulation together with the macroscopic image is illustrated in Fig. 9.

Thanks to the selected matching filler material, the weld has nearly the same hardness as the base material, while slight (10%) softening can be observed in the heat-affected zone.

Five hardness measurements were taken on the cross sections at the thermocouples of the Gleeble specimens. The average hardness results with the standard deviations are shown in Fig. 10. Compared to the 233 ± 1.5 HV10 base material and the 233 ± 2.2 HV10 original weld, slight hardening can be observed in the investigated HAZ subzones; however, the measured 265 HV10 peak hardness is safely under the permitted 380 HV10 value due to the mostly AF microstructure. The medium ($t_{8/5} = 15$ s) cooling time resulted in equal hardness with the base material and the weld. In the case of the examined HAZ zones, a decreasing trend in hardness can be observed as the cooling time increases. With faster cooling, the probability for bainitic features increases. Microstructural features resembling upper bainite were observed in CGHAZ-W with $t_{8/5} = 5$ s (Fig. 7a), which is connected to the increased hardness in samples simulated with faster cooling rate.

3.3 Instrumented Charpy V-notch impact toughness test

The Charpy V-notch (CVN) impact toughness tests were performed on a PSD 300 instrumented impact tester. During the evaluation, it was taken into account that the required impact energy of the S500ML base material is 20 J at − 40 °C according to EN 10025–4 [15]. Based on the diagram in Fig. 11, due to the AF microstructure, both the original weld and the examined HAZ subzones safely exceeded this relatively low requirement for impact energy. Compared to ferrite-pearlite and martensitic structural steels, the HAZ subzones of S500ML are significantly more ductile. Unlike the typical case of CGHAZ in base material [22], CGHAZ-W results in the highest toughness among the investigated zones. In the case of ICHAZ-W and ICCGHAZ-W, the impact energy decreased with the increasing cooling time, although this tendency was not observed in CGHAZ-W. Based on the fracture surface analysis, the original weld and

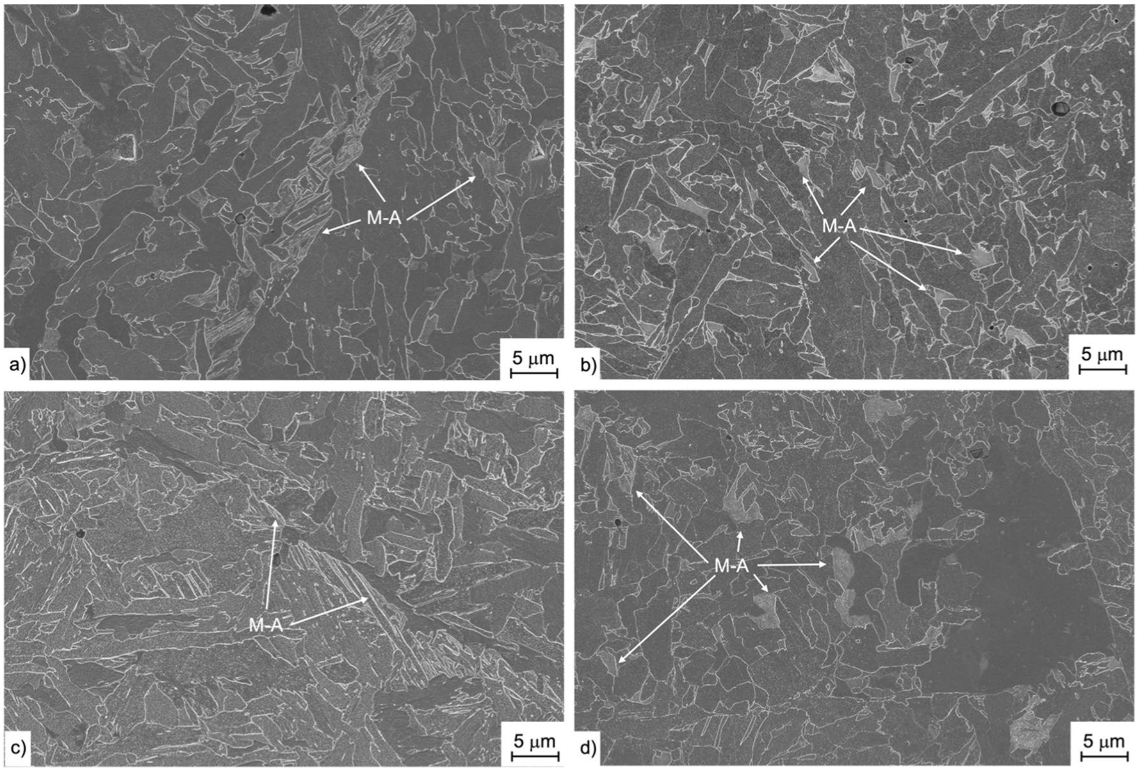

Fig. 8 Scanning electron microscope images of ICHAZ-W with $t_{8/5}=5$ (**a**) and 30 s (**b**) and ICCGHAZ-W with $t_{8/5}=5$ s (**c**) and 30 s (**d**) showing the M-A constituents in the microstructure

Fig. 9 Macroscopic image of the original single-pass weld and its hardness distribution before the Gleeble simulation

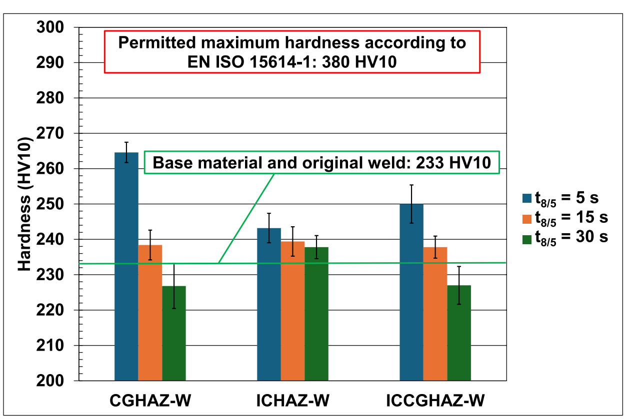

Fig. 10 Hardness of the simulated HAZ subzones

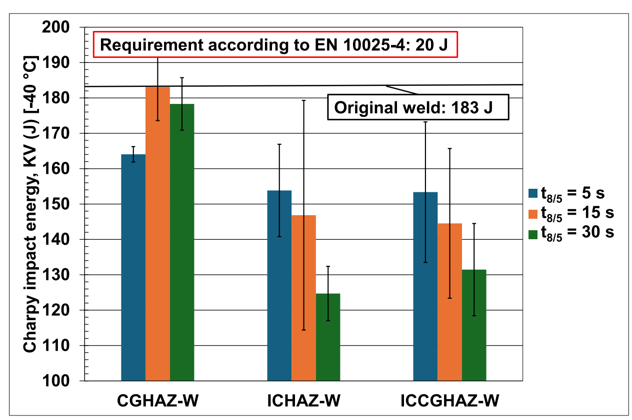

Fig. 11 The Charpy impact energy of simulated HAZ-W subzones at – 40 °C

the CGHAZ-W were ductile, while ICHAZ-W and ICCGHAZ-W showed ductile–brittle characteristics. The ratio of brittle parts was the highest in ICHAZ-W.

The reason for the differing impact toughness results can be explained by the microstructures. In CGHAZ-W, the microstructure remained mainly AF, as in the original weld. Therefore, the toughness did not decrease significantly. A slight decrease was seen in case of $t_{8/5} = 5$ s, which can be attributed to the formation of bainitic-looking features (Fig. 7a) and the consequent increase in hardness (Fig. 10).

In ICHAZ-W, the most significant phenomenon in the microstructure is the formation of M-A constituents, which are known to reduce toughness in steels [4]. Therefore, as a result of increasing fraction of M-A along with the increasing cooling time (Fig. 8a and b), the impact toughness also decreased steadily in ICHAZ-W samples when the cooling time increased.

ICCGHAZ in base material is usually the weakest spot in welded joints [4]. However, in case of weld metal, both the CGHAZ-W and unaffected weld metal have fairly similar microstructures, being mainly AF. Consequently, ICHAZ-W and ICCGHAZ-W cycles produce also fairly similar microstructures, including the fraction of M-A, which is mainly affected by the cooling time. In comparison to base material HAZ, the starting microstructures are different in ICHAZ and ICCGHAZ, and therefore ICCGHAZ typically has lower toughness due to coarse grains and M-A. The similarities of ICHAZ-W and ICCGHAZ-W and also the increasing fraction of M-A in both HAZ-Ws along with the increasing cooling time can be checked in Fig. 8.

Figure 12 shows the macroscopic images of the fracture surfaces of the tested CVN specimens and a closer look at the fracture surface of the original weld and ICCGHAZ-W with $t_{8/5} = 30$ s is provided in Fig. 13. The original weld showed mainly ductile fracture behavior, and this is evident in the fractographies in Fig. 13a and b. However, regions of brittle facture are present also in the original weld, which could be attributed to the presence of grain boundary ferrite among the mostly AF microstructure. As seen in Fig. 13b, a secondary crack was spotted in one of these brittle regions. Similar observations were made by Kang et al. [11], who concluded that the grain boundary ferrite regions in the otherwise AF microstructure are the weakest locations in a low hardenability weld metal with similar composition to that in the present study. Fractographies in Fig. 12c and d are taken from the ICCGHAZ-W sample with $t_{8/5} = 30$ s. This particular sample was one of the most brittle among the tested samples, showing absorbed impact energy of only 120.1 J. Therefore, the fracture surface was full of brittle fracture regions with only few ductile fracture regions appearing between them.

The relationship between expansion and Charpy impact energy is illustrated in Fig. 14. The expansion varied between 1.5 and 2.5 mm, indicating favorable toughness properties.

Compared to the conventional Charpy V-notch impact toughness test, where the whole energy absorbed during the fracture is determined, instrumented impact testing can provide more detailed information about the fracture process and the ductile/brittle behavior of the material. Using strain gauge

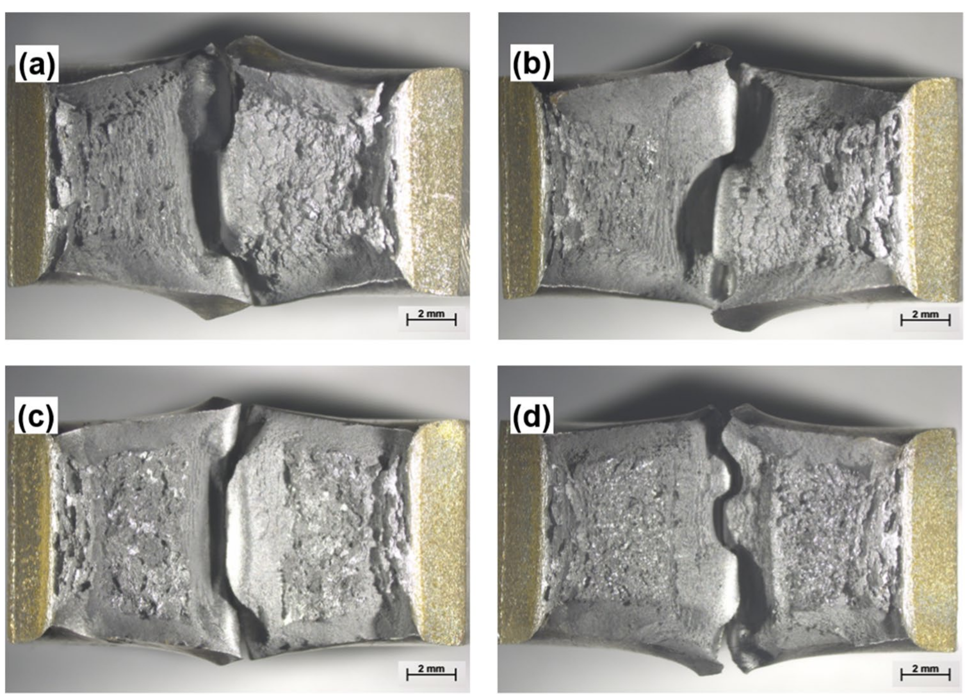

Fig. 12 Macroscopic images of the fracture surface of impact test specimens: **a** original weld, **b** CGHAZ-W $t_{8/5} = 15$ s, **c** ICHAZ-W $t_{8/5} = 15$ s, and **d** ICCGHAZ-W $t_{8/5} = 15$ s

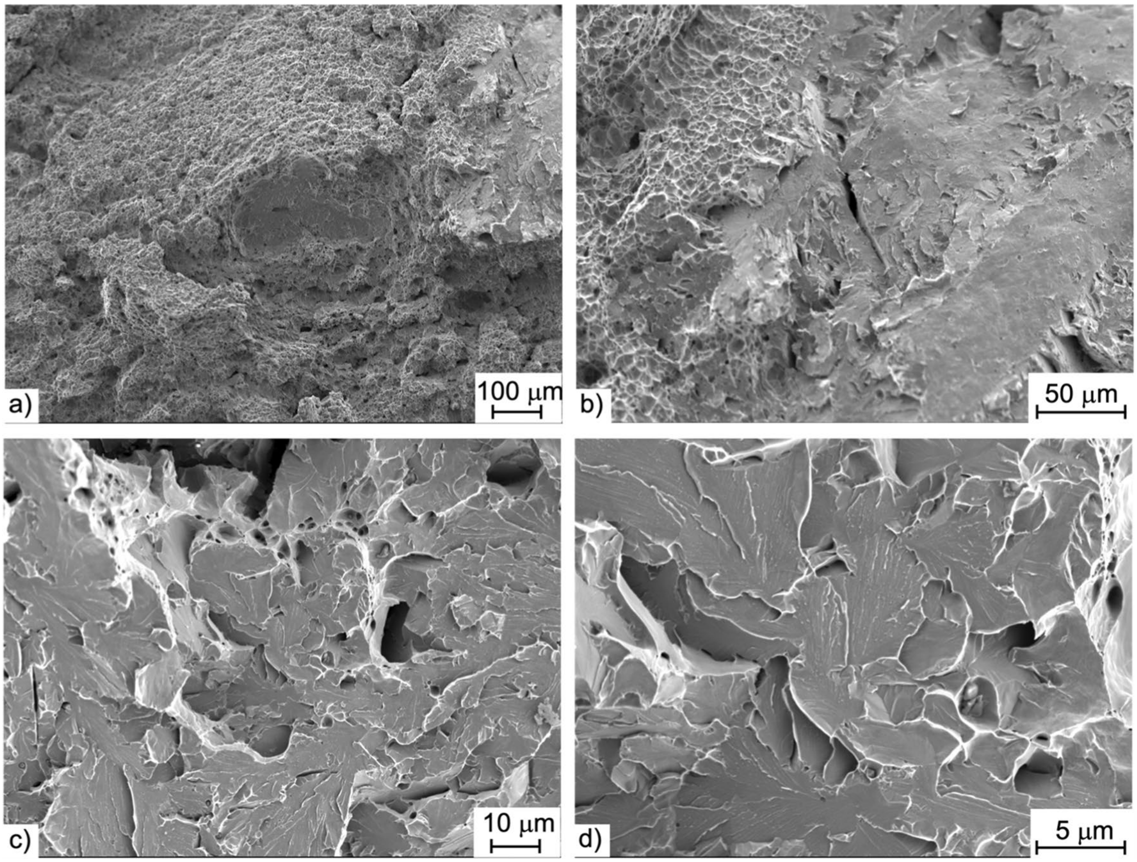

Fig. 13 Scanning electron microscope images of the fracture surface of impact test specimens: **a**, **b** original weld, **c**, **d** ICCGHAZ-W $t_{8/5} = 30$ s

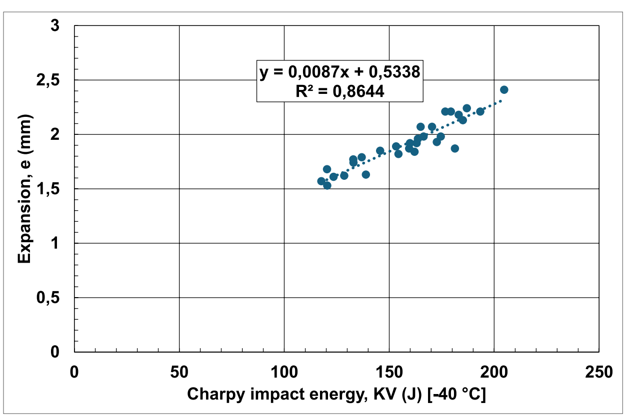

Fig. 14 Expansion in the function of Charpy impact energy

measurement technology, the load-time diagram can be determined, and the characteristic points of the fracture process can be identified (the start of the plastic strain, maximal force, start of the unstable crack propagation, end of the unstable crack propagation) [23]. In the registered diagram, the unstable crack propagation stage is correlated with the amount of brittle fracture on the fracture surface. From the load-time diagram, the force–displacement diagram can be calculated. Assuming that the crack initiation occurs at the maximal force, the registered diagram can be divided into two parts according to the maximal force. Up to the maximum force, the area under the curve is considered the absorbed energy for crack initiation (W_i), while the remaining area is for crack propagation (W_p). As the ratio of the absorbed energy for the crack initiation increases, the toughness of the examined material decreases [23]. The detailed method for the instrumented Charpy V-notch pendulum impact test is described in EN ISO 14556 [24]. During the instrumented Charpy V-notch impact tests, force–displacement diagrams were determined for the unaffected weld metal and the simulated HAZ subzones. Figure 15 shows the force–displacement diagram of the original weld metal and diagrams for the simulated HAZ subzones for the $t_{8/5} = 15$ s. In the case of the original weld and the CGHAZ-W, the diagrams show typical ductile behavior, while the diagrams of ICHAZ-W and ICCGHAZ-W are narrower, indicating ductile–brittle characteristics due to the observed unstable crack propagation. In connection with the similar hardness of the different zones, the measured maximum force values are also nearly the same. The measured and

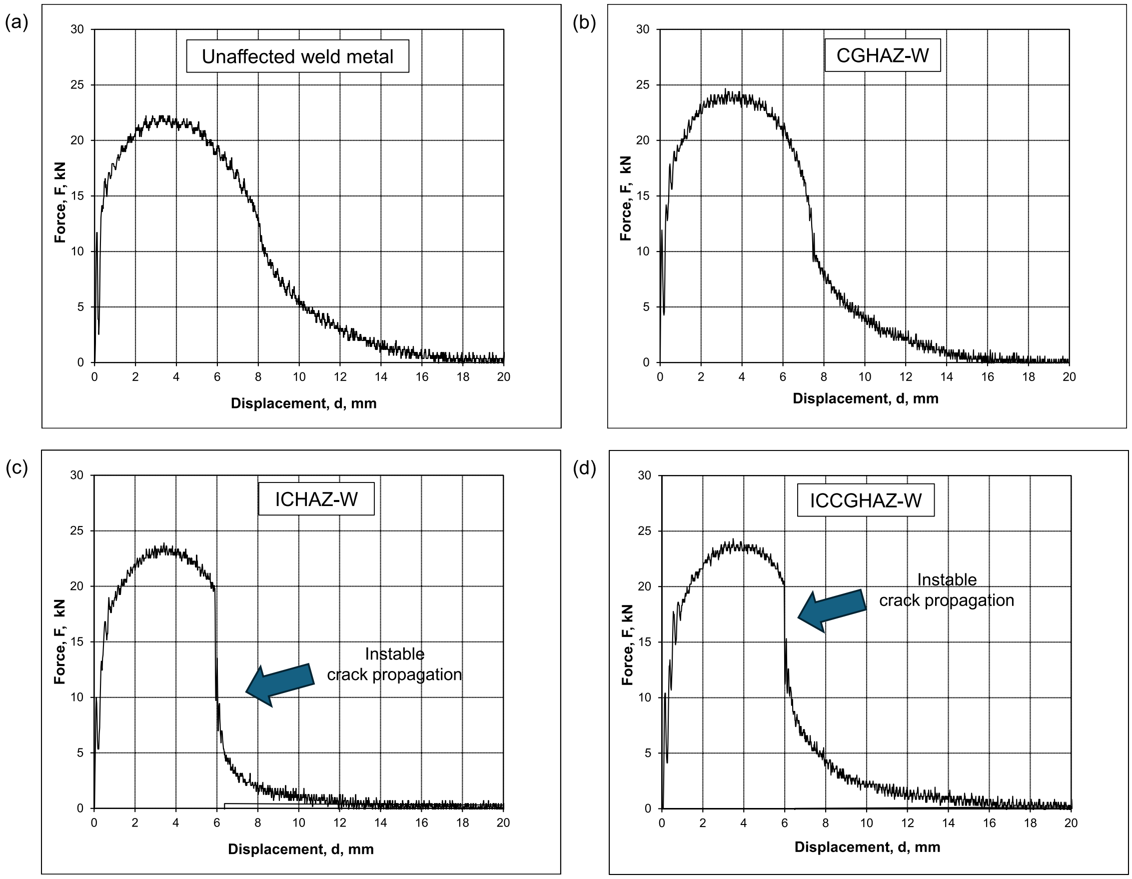

Fig. 15 Determined Force–Displacement diagrams during instrumented impact testing: **a** original weld metal, **b** CGHAZ-W, **c** ICHAZ-W, and **d** ICCGHAZ-W, $t_{8/5} = 15$ s

calculated data of the Charpy V-notch impact toughness test are summarized in Table 3.

On the basis of the material tests carried out, it can be concluded that thanks to the AF weld microstructure, even the HAZ subzones considered critical in terms of toughness are acceptable; they show a toughness significantly exceeding the standard requirement (20 J at – 40 °C), and also the degree of hardening and softening can be considered minimal. However, despite the relatively high impact energy values, unstable crack propagation occurred in ICHAZ-W and ICCGHAZ-W, indicating ductile–brittle behavior. Increasing the $t_{8/5}$ cooling time also reduces the hardness of the HAZ-W subzones formed in the weld and the toughness of the ICHAZ-W and ICCGHAZ-W; therefore, overall, it is advisable to weld these steels with a low welding heat input.

Table 3 Measured and calculated data of instrumented Charpy V-notch impact test

Zone	T_{max}, °C	$t_{8/5}$, s	F_{max}, kN	e, mm	CVN, J	W_i, J	W_{ic}, %	W_p, J	W_{pc}, %	Fracture mode
BM	-	-	22.7	2.23	183.4	55.5	30.6	126.7	69.4	Mostly ductile
CGHAZ-W	1350	5	26.5	1.93	164.1	56.4	34.4	107.6	65.6	Mostly ductile
		15	24.8	2.02	183.1	62.0	33.9	121.0	66.1	Mostly ductile
		30	23.3	2.14	178.3	66.9	37.5	113.4	62.5	Little instable crack propagation
ICHAZ-W	815	5	24.2	1.80	153.8	59.3	38.9	94.6	61.1	Little instable crack propagation
		15	23.9	1.83	146.8	67.1	46.2	79.7	53.8	Ductile–brittle
		30	23.1	1.65	124.7	54.2	37.7	72.9	57.3	Ductile–brittle
ICCGHAZ-W	1350 815	5	24.9	1.83	153.4	61.0	40.2	92.5	59.8	Little instable crack propagation
		15	24.0	1.83	144.5	62.4	43.0	82.1	57.0	Ductile–brittle
		30	23.9	1.73	131.5	80.6	61.0	50.6	39.0	Brittle-ductile

4 Conclusions

Physical simulation experiments were carried out on S500ML shipbuilding steel for the analysis of the effect of multipass welding on weld properties. The main findings of the research work are summarized as follows:

1. With the help of physical simulation, it was possible to produce HAZ subzones critical to toughness in the multi-layer weld seam of the examined steel, which were as follows: coarse-grained heat-affected zone (CGHAZ-W), intercritical heat-affected zone (ICHAZ-W), and intercritically reheated coarse-grained zone (ICCGHAZ-W).
2. Significant hardening and softening were not observed in the examined CGHAZ-W, ICHAZ-W, or ICCGHAZ-W. The $t_{8/5} = 15$ s resulted in nearly equal hardness with the original weld and base material.
3. Mainly acicular ferrite (AF) was observed in simulated HAZ-W subzones formed in the weld, although grain boundary ferrite and ferrite side plates were also present. Slight hardening occurred in CGHAZ-W at fast cooling ($t_{8/5} = 5$ s) producing bainitic features, and M-A constituents formed due to the ICHAZ-W and ICCGHAZ-W thermal cycles.
4. The toughness of the original weld metal and the simulated HAZ-W subzones formed in the weld significantly exceeded the base material requirement, with more than 100 J impact energy at − 40 °C.
5. The measured impact toughness energy of the examined HAZ-W subzones formed in the weld was under the original weld toughness in all cases. In CGHAZ-W, the impact toughness energy decreased only slightly, and the cooling time did not have a significant role. In ICHAZ-W and ICCGHAZ-W, the longer $t_{8/5}$ cooling time resulted in lower impact toughness energy due to the increased time for carbon partitioning from matrix to M-A constituents, which led to an increasing fraction of M-A in the microstructure. Overall, ICHAZ-W showed the lowest toughness among all subzones, which was indicated by relatively large unstable crack propagation in the impact energy diagrams.
6. In addition to M-A constituents, upper bainite and grain boundary ferrite were suggested to have been contributed to the decreased impact toughness in the otherwise mainly AF microstructures.

Funding Open Access funding provided by University of Oulu (including Oulu University Hospital). The financial support of the János Bolyai Research Scholarship of the Hungarian Academy of Sciences (Grant number: Bo/00643/22/6) and Business Finland, in project Fossil-Free Steel Applications: Phase II (Grant number: Dnro 5562/31/2023) is gratefully acknowledged.

Declarations

Competing interests The authors declare no competing interests.

References

1. Gáspár M, Sisodia R, Tervo H, Javaheri V, Kaijalainen A (2023) Challenges and opportunities in the arc welding of offshore steels. In: Wei Z, Pang J (eds) Proceedings of the 76th IIW Annual Assembly and International Conference on Welding and Joining, Singapore, pp. 567–574. Paper: OR-11–0211
2. Bhadeshia H, Honeycombe R (2017) Steels: Microstructure and Properties, 4th edn. Netherlands, Elsevier, Amsterdam
3. Tervo H, Kaijalainen A, Pallaspuro S, Anttila S, Mehtonen S, Porter D, Kömi J (2020) Low-temperature toughness properties of 500 MPa offshore steels and their simulated coarse-grained heat-affected zones. Mat Sci Eng A 773:138719. https://doi.org/10.1016/j.msea.2019.138719
4. Nevasmaa P (1996) Evaluation of HAZ toughness properties in modern low carbon low impurity 420, 550 and 700 MPa yield strength thermomechanically processed steels with emphasis on local brittle zones. University of Oulu, Lisensiaatintyö, p 176
5. Handbook M (1995) Volume 6, Welding, brazing and soldering. ASM International, USA
6. Wilhelm E, Mente T, Rhode M (2021) Waiting time before NDT of welded offshore steel grades under consideration of delayed hydrogen-assisted cracking. Weld World 65:947–959. https://doi.org/10.1007/s40194-020-01060-5
7. Tervo H, Kaijalainen A, Javaheri V, Kolli S, Alatarvas T, Anttila S, Kömi J (2020) Characterization of coarse-grained heat-affected zones in Al and Ti-deoxidized offshore steels. Metals 10:1096. https://doi.org/10.3390/met10081096
8. EN 10225–1 (2020) Weldable structural steels for fixed offshore structures. Technical delivery conditions. Part 1: Plates
9. Tervo H, Kaijalainen A, Javaheri V, Ali M, Alatarvas T, Mehtonen S, Anttila S, Kömi J (2021) Comparison of impact toughness in simulated coarse-grained heat-affected zone at Al-deoxidized and Ti-deoxidized offshore steels. Metals 11:1783. https://doi.org/10.3390/met11111783
10. Seo JS, Seo K, Kim HJ (2014) Effect of titanium content on weld microstructure and mechanical properties of bainitic GMA welds. Weld World 58:893–901. https://doi.org/10.1007/s40194-014-0168-1
11. Kang Y, Park G, Jeong S, Lee C (2018) Correlation between microstructure and low-temperature impact toughness of simulated reheated zones in the multi-pass weld metal of high-strength

steel. Metall Mater Trans A 49:177–186. https://doi.org/10.1007/s11661-017-4384-3
12. Nellikode S, Manladan SM, Jo I, Jung S-J, Kim I-C, Park H, Nam D-G, Park Y-D (2023) Effect of microstructural heterogeneities on variability in low-temperature impact toughness in multi-pass weld metal of 420 MPa offshore engineering steel. Weld World 67:1679–1693. https://doi.org/10.1007/s40194-023-01521-7
13. Bhole SD, Nemade JB, Collins L, Liu C (2006) Effect of nickel and molybdenum additions on weld metal toughness in a submerged arc welded HSLA line-pipe steel. Journal of Mat Proc Techn 173(1):92–100. https://doi.org/10.1016/j.jmatprotec.2005.10.028
14. Abson DJ (2018) Acicular ferrite and bainite in C-Mn and low-alloy steel arc weld metals. Sci Techn of Weld and Join 23(8):635–648. https://doi.org/10.1080/13621718.2018.1461992
15. EN 10025–4 (2023) Hot rolled products of structural steels. Part 4: Technical delivery conditions for thermomechanical rolled weldable fine grain structural steels
16. EN ISO 14171 (2016) Welding consumables. Solid wire electrodes, tubular cored electrodes and electrode/flux combinations for submerged arc welding of non alloy and fine grain steels. Classification
17. Adonyi Y (2006) Heat-affected zone characterization by physical simulations. Weld Jour 85(10):42–47
18. Zs K, Gy N, Lukács J (2022) Fracture mechanical analysis of gleeble simulated heat affected zones in high strength steels. Peri Poly Mech Eng 66(1):83–89. https://doi.org/10.3311/PPme.19077
19 Rykalin NN (1953) Teplovie processzi pri szvarke, Vüpuszk 2. Izdatelsztvo Akademii, Nauk SzSzSzR, Moscow, p 56
20. EN ISO 15614–1 (2017) Specification and qualification of welding procedures for metallic materials. Welding procedure test. Part 1: Arc and gas welding of steels and arc welding of nickel and nickel alloys
21. CEN ISO/TR 15608 (2021) Welding. Guidelines for a metallic materials grouping system
22. Tervo H, Mourujärvi J, Kaijalainen A, Kömi J (2018) Mechanical properties in the physically simulated heat-affected zones of 500 MPa offshore steel for arctic conditions. In: Jármai K, Bolló B (eds) Vehicle and Automotive Engineering 2. VAE 2018, Lect Not in Mech Eng, Springer. https://doi.org/10.1007/978-3-319-75677-6_66
23. Lenkeyné B Gy, Winkler S, Tóth L, Blauel JG (1997 September) Investigations on the brittle to ductile fracture behaviour of base metal, weld metal and HAZ material by instrumented impact testing. In Proceedings of the 1st International Conference on Welding Technology, Materials and Material Testing, Fracture Mechanics and Quality Management, Wien, Austria, 22–24, pp. 423–432
24. EN ISO 14556 (2023) Metallic materials. Charpy V-notch pendulum impact test. Instrumented test method